

Structural and conductivity studies of $\text{LiNi}_{0.5}\text{Mn}_{0.5}\text{O}_2$ cathode materials for lithium-ion batteries

N. MURALI^{1*}, K. VIJAYA BABU¹, K. EPHRAIM BABU², V. VEERAI AH²

¹Advanced Analytical Laboratory, Andhra University, Visakhapatnam-530003, India

²Department of Physics, Andhra University, Visakhapatnam-530003, India

Layered oxide LiMO_2 (Ni, Co, Mn) have been proposed as cathode materials for lithium-ion batteries. Mainly LiNiO_2 is accepted as an attractive cathode material because of its various advantages such as low cost, high discharge capacity, good reversibility. The $\text{LiNi}_{0.5}\text{Mn}_{0.5}\text{O}_2$ powders are synthesized by a sol-gel method using citric acid as a chelating agent. The structure of the synthesized material is analyzed by using XRD, FT-IR and the microstructures of the samples are observed by using FESEM. The intensities and positions of the peaks are in a good agreement with the previous results. The morphological changes are clearly observed as a result of manganese substitution. The Fourier transform infrared (FT-IR) spectra obtained with KBr pellet data reveal the structure of the oxide lattice constituted by LiO_6 and NiO_6 octahedra. The conductivity studies are characterized by (EIS) in the frequency range of 42 Hz to 1 MHz at room temperature to 120 °C. The dielectric properties are analyzed in the framework of complex dielectric permittivity and complex electric modulus formalisms. It indicates that the conductivity increases with increasing temperature. The fitting data of EIS plots replicate the non-Debye relaxation process with negative temperature coefficient of resistance (NTCR) behavior.

Keywords: *layered structure; FESEM; impedance; electric modulus*

© Wrocław University of Technology.

1. Introduction

The layered structure cathode materials LiMO_2 (M = Co, Ni and Mn) are intensively studied, because of their high energy density, large discharge capacity and low cost [1–3]. In general, cathode materials are characterized by high oxidation potential, long cycle life, good reversibility of reaction, good electronic and ionic conductivity; they are non-soluble in electrolytes and structurally stable for repeated charging/discharging processes [4, 5]. The LiCoO_2 has been the most widely used cathode material in commercial lithium ion batteries. However, it causes many problems such as high toxicity, high cost, low practical capacity, etc. [6–8]. Therefore, alternate cathode materials with low cost and non-toxicity have been studied in recent years. LiNiO_2 is superior to LiCoO_2 due to its low cost and toxicity in high power and large scale energy storage applications, such

as mobile phones, laptops and electric tools. So, LiNiO_2 is a promising alternative to LiCoO_2 . Studies on cationic substitution, including Fe, Mn, Al, Mg, Co/Al and Co/Mg for Ni are an attempt to stabilize the layered structure of the material [9–15]. In the electronic stabilization approach, Mn is partially substituted by Ni in equal concentration, such as 1:1 in $\text{LiNi}_{0.5}\text{Mn}_{0.5}\text{O}_2$ compound. Ni is found to be at +2 oxidation state and Mn at +4 oxidation state, thus eliminating the adverse effects of Jahn-Teller distortion prone Mn^{3+} ions. The sol-gel method, solid-state reaction method, co-precipitation method, combustion method and emulsion method have been reported for the synthesis of $\text{LiNi}_{0.5}\text{Mn}_{0.5}\text{O}_2$ [16–18]. Among all the methods used for the synthesis of $\text{LiNi}_{0.5}\text{Mn}_{0.5}\text{O}_2$, the sol-gel method has some advantages such as good stoichiometric control, production of sub-micronized particles and lower calcination temperature.

In this work, the sol-gel method has been used for the synthesis of $\text{LiNi}_{0.5}\text{Mn}_{0.5}\text{O}_2$ cathode

*E-mail: muraliphda@gmail.com

materials at 800 °C for 20 hours and the obtained compound has been systematically characterized. The main emphasis has been focused on the study of conduction mechanism and dielectric behavior. From the conductivity studies, various important parameters such as activation energy, modulus, relative dielectric constant, etc., were estimated and the results were discussed.

2. Experimental

$\text{LiNi}_{0.5}\text{Mn}_{0.5}\text{O}_2$ cathode materials were synthesized by using sol-gel method, from stoichiometric amounts of $\text{CH}_3\text{COOLi}\cdot 2\text{H}_2\text{O}$ (AR), $\text{Ni}(\text{NO}_3)_2\cdot 6\text{H}_2\text{O}$ (AR) and $\text{C}_4\text{H}_6\text{MnO}_4\cdot 4\text{H}_2\text{O}$ (AR) which were dissolved in distilled water. The aqueous solution of citric acid, which was acting as a chelating agent, was added to the mixture of the metal ion solution according to their molar ratio of 1:1. At the same time, an ammonia solution, as a precipitation agent was separately added. The reaction temperature was kept at 80 °C and pH was controlled by ammonia solution to the value of 8 to 9. The solutions were added together under stirring at 130 °C for 10 hours, forming sol solution. The sol solution was vaporized at 130 °C till the dry gel was formed, followed by the heat treatment at 500 °C for 6 h in air with a 5 °C/min heating rate to eliminate the organic residues. The powders were thoroughly ground and then calcined at 800 °C for 20 hours in air to obtain the required compounds. The powder samples added with polyvinyl alcohol (PVA) as a binder were ground and then pressed at 5 tons pressure for 6 minutes into a circular disk shaped pellet. The pellet was then sintered at 800 °C for 20 h in air at heating and cooling rates of 5 °C/min. The surface layers of the sintered pellet were carefully polished and washed with acetone and then the pellet was coated with silver paste on the opposite faces, which acted as electrodes.

The powder X-ray diffraction (XRD) data of the sample were collected on a Rigaku $\text{CuK}\alpha$ diffractometer with diffraction angles of 20° to 80° in increments of 0.02°. The unit cell lattice parameter was obtained by the least square fitting method from the d-spacing and (h k l) values. Further,

the crystallite size of the sample was obtained from XRD pattern by applying Scherrer's equation. The particle morphology of the powder was observed using a field effect scanning electron microscopy image taken from Carl Zeiss, EVOMA 15, Oxford Instruments, Inca Penta FETx3.JPG. Fourier transform infrared (FT-IR) spectra were obtained on a Shimadzu FT-IR-8900 spectrometer using a KBr pellet technique in the wave number range between 350 cm^{-1} and 800 cm^{-1} . The impedance study was performed by a Hioki 3532-50 LCR Hitester in the frequency range of 42 Hz to 1 MHz at the temperature range from room temperature to 120 °C.

3. Results and discussion

3.1. XRD analysis

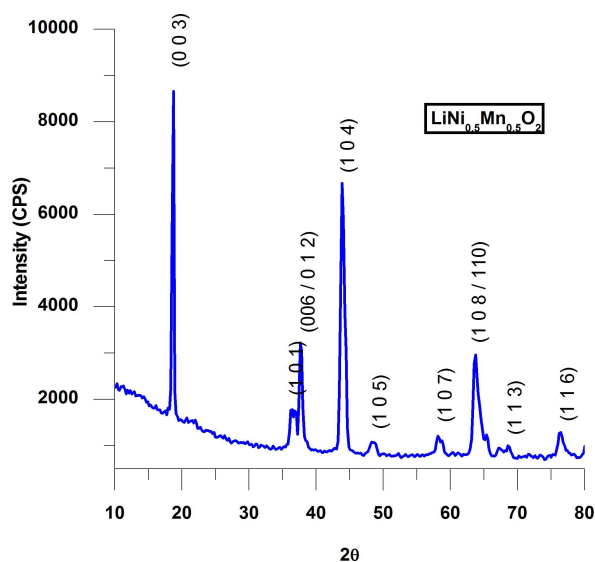
The XRD spectrum of the $\text{LiNi}_{0.5}\text{Mn}_{0.5}\text{O}_2$ material prepared by sol-gel method at 800 °C for 20 hours is shown in Fig. 1. The XRD spectrum can be indexed based on the $\alpha\text{-NaFeO}_2$ structure with a space group $R\bar{3}m$ [19, 20]. The existence of doublet XRD peaks at around 38° and 64° for $I_{(006)}/I_{(102)}$ and $I_{(108)}/I_{(110)}$, clearly splitted, indicates a layered structure of the sample. The intense peaks corresponding to the planes (0 0 3), (1 0 1) and (1 0 4) suggests a well layered structure. The lattice cell properties were calculated by using of Unit-Cell software (1995) [21]. The structural parameters of $\text{LiNi}_{0.5}\text{Mn}_{0.5}\text{O}_2$ are provided in Table 1. The intensity ratio of (0 0 3)/(1 0 4) planes (I_{003}/I_{104}) is an indicator of the degree of displacement of ions between lithium layers at 3a site and transition metal layers at 3b site and is called as cation mixing disorder [22–24]. The low intensity value of I_{003}/I_{104} is an indicator of high cation disorder which leads to poor electrochemical performance of a battery. The crystallite size obtained using the Scherrer's equation for (0 0 3) peak was 1.9526 nm.

The structure of lattice parameters for $\text{LiNi}_{0.5}\text{Mn}_{0.5}\text{O}_2$ of the synthesized compound is shown in Table 1. The intensity ratio of $I_{(003)}/I_{(104)}$ is 1.49, which is a qualitative measure of the better battery performance of the synthesized compound [25, 26]. The c/a value for the $\text{LiNi}_{0.5}\text{Mn}_{0.5}\text{O}_2$ is > 4.94 indicating that

Table 1. Lattice parameter, unit cell volume, I_{003}/I_{104} and R-factor of $\text{LiNi}_{0.5}\text{Mn}_{0.5}\text{O}_2$ sample.

Compound	a [Å]	c [Å]	c/a	Cell volume [Å] ³	I_{003}/I_{104}	R-factor ($(I_{006}+I_{102})/I_{101}$)	Crystallite size [nm]
$\text{LiNi}_{0.5}\text{Mn}_{0.5}\text{O}_2$	2.8798	14.3406	4.9797	102.9982	1.4891	0.20598	1.9526
$\text{LiNi}_{0.5}\text{Mn}_{0.5}\text{O}_2$ [25, 26]	2.887	14.262	4.94	118.87	–	–	–

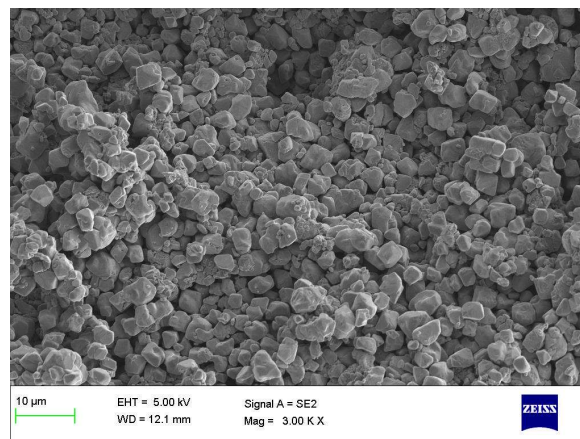
the phases possess the hexagonal layer structure, similar to pristine LiNiO_2 [27–29]. It was also found that the density of the sintered pellet is 82 % of the theoretical density.

Fig. 1. XRD pattern of $\text{LiNi}_{0.5}\text{Mn}_{0.5}\text{O}_2$ prepared by sol-gel method.

3.2. FESEM analysis

Fig. 2 shows the FESEM photographs of the synthesized $\text{LiNi}_{0.5}\text{Mn}_{0.5}\text{O}_2$ cathode material. The FESEM image reveals that the material is comprised of well crystallized particles with no obvious aggregation and well-shaped, smooth crystals with sharp edges morphology [30–33]. As seen in Fig. 2 the aggregated particles of the material are spherical in shape, having a diameter of 10 μm . The cathode powders prepared from the spray solution without additives have irregular morphologies. Since we have been interested in the structural changes of the cathode material upon

electrochemical cycling therefore these important steps were thoroughly studied [34–36].

Fig. 2. FESEM image of $\text{LiNi}_{0.5}\text{Mn}_{0.5}\text{O}_2$ powder.Table 2. FT-IR wavenumbers variation of $\text{LiNi}_{0.5}\text{Mn}_{0.5}\text{O}_2$ sample.

Source	Wavenumbers [cm^{-1}]			
authors	421.4644	477.4024	512.0154	615.248
[37]	–	474	532	597

3.3. FT-IR analysis

The mode of vibrations for $\text{LiNi}_{0.5}\text{Mn}_{0.5}\text{O}_2$ in the regions between 400 cm^{-1} to 1200 cm^{-1} is depicted in Fig. 3. The FT-IR spectra show the local structure of the oxide lattice constituted by LiO_6 and MO_6 octahedral [37]. The peaks at 512 and 615 cm^{-1} are the bending modes of Ni–O in MO_6 , and the band at around 431 cm^{-1} can be assigned to the asymmetric stretching of Li–O in LiO_6 environments [38, 39]. The FT-IR wavenumber variations of the compound are listed in Table 2. All the values are in good correlation with the previous results.

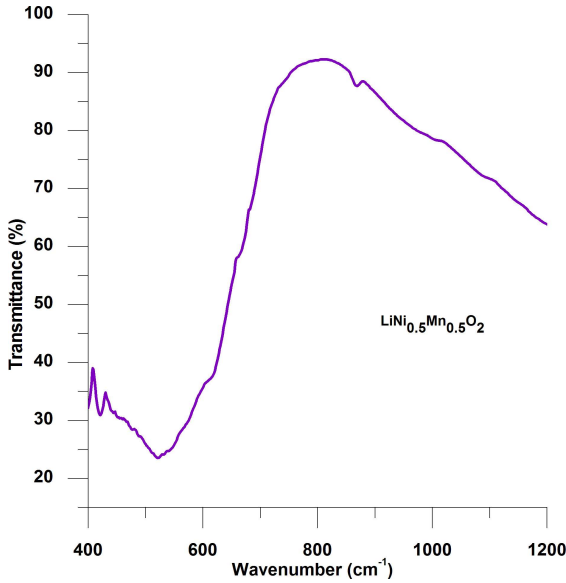


Fig. 3. FT-IR graph of $\text{LiNi}_{0.5}\text{Mn}_{0.5}\text{O}_2$ sample.

3.4. Electrical impedance studies (EIS)

In impedance technique, the real and imaginary parts of the impedance of a sample are measured simultaneously as a function of frequency. The measured impedance data can be represented in different forms, using the interrelations as follows:

Complex impedance

$$Z^* = Z' - jZ'' \quad (1)$$

Complex modulus

$$M^* = M' + jM'' = j\omega C_0 Z^* \quad (2)$$

where $j = \sqrt{-1}$, C_0 is the vacuum capacitance and $\omega = 2\pi f$ is the angular frequency.

On the Nyquist plot shown in Fig. 4, Z' is the real part of the impedance and Z'' is the imaginary part of the impedance. Each semicircular arc begins from lower frequency to the right direction of the Z' -axis and ends in the left direction of Z'' -axis at higher frequencies. The obtained curves appear in the form of single semicircles with small spikes at lower frequencies and the depressed semicircles correspond to the bulk conduction, whereas the small spikes are due to the electrode polarization. The proposed system has semicircular Argand plots with the center located below the real

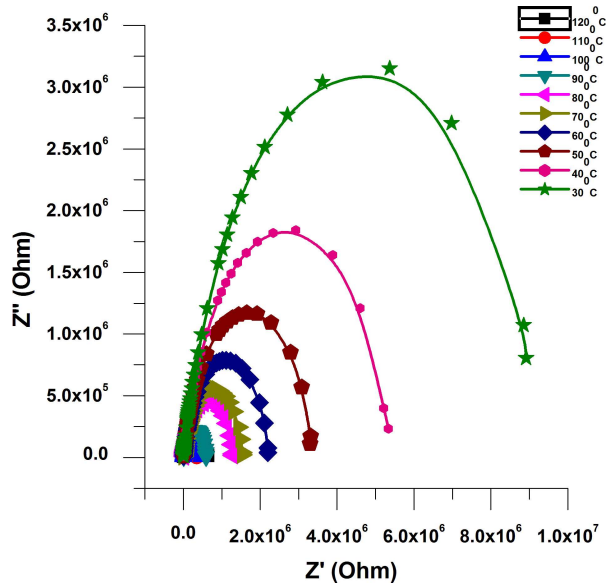


Fig. 4. Nyquist plots for $\text{LiNi}_{0.5}\text{Mn}_{0.5}\text{O}_2$ material at different temperatures.

axis, precisely indicating the non-Debye relaxation process [40].

Fig. 5a and Fig. 5b show the variation of real and imaginary parts of impedance Z' and Z'' of the synthesized sample as a function of frequency at different temperatures. It is observed that the Z' and Z'' values are typically higher at lower frequency regions for different temperatures. The asymmetric broadening of the peaks with an increase in temperature suggests the presence of electrical process in the material with a distribution of relaxation time. This indicates the temperature dependence of electrical relaxation phenomena in the materials [41]. The high value of Z' and Z'' at lower frequency regions is due to the higher polarization caused by space charge. It is also observed that the values of Z' and Z'' gradually decrease with increasing frequency and temperature. This indicates an increase in AC conductivity with the rise in temperature and frequency. Here, at low frequency, the value of Z' decreases with the rise in temperature showing negative temperature coefficient of resistance (NTCR) type behavior, similar to semiconductors [42].

The AC conductivity is a very important property of a cathode material. For a better charge transfer process during lithium

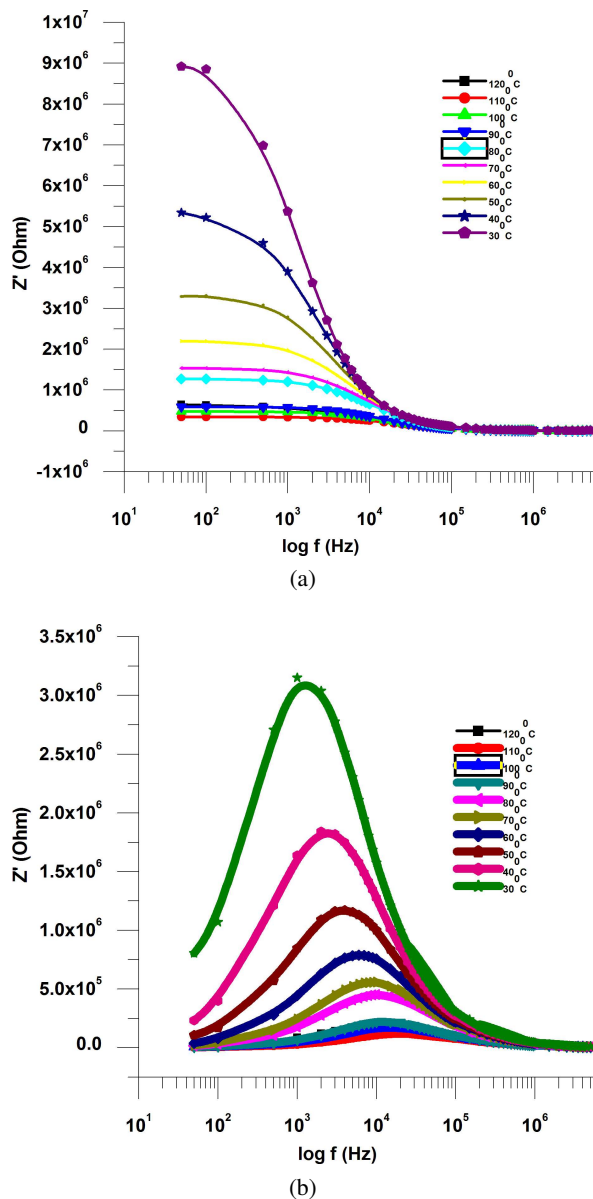


Fig. 5. (a) real and (b) imaginary part of impedance of $\text{LiNi}_{0.5}\text{Mn}_{0.5}\text{O}_2$ material as a function of frequency at different temperatures.

intercalation-deintercalation in a lithium-ion cell, conductivity plays a significant role. The bulk conductivity has been calculated at various temperatures using the bulk resistance obtained from the analyzed impedance data and the pellet dimensions of the compound. The bulk conductivity (σ) value is calculated using the formula:

$$\sigma = \frac{L}{R_b A} S/cm \tag{3}$$

where R_b is the bulk resistance of the sample, L is the thickness of the pellet, A is the effective area.

Fig. 6 shows the variation of AC conductivity of the synthesized material as a function of frequency at different temperatures (30 °C to 120 °C). At low frequency, AC conductivity exhibits dispersion and increases with an increase in frequency and temperature [43]. The maximum AC conductivity of the synthesized sample is 1.03×10^{-6} S/cm at 60 °C.

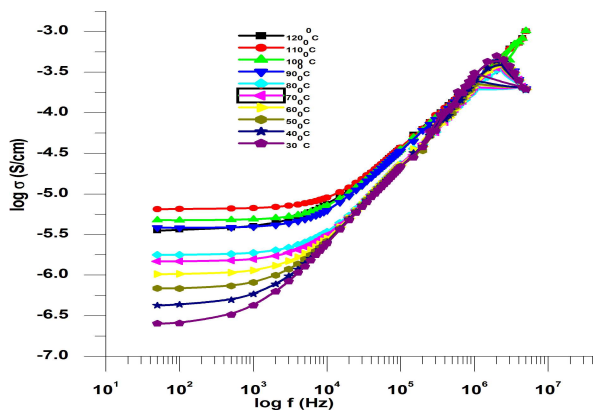


Fig. 6. Variation of AC conductivity of $\text{LiNi}_{0.5}\text{Mn}_{0.5}\text{O}_2$ material as a function of frequency at different temperatures.

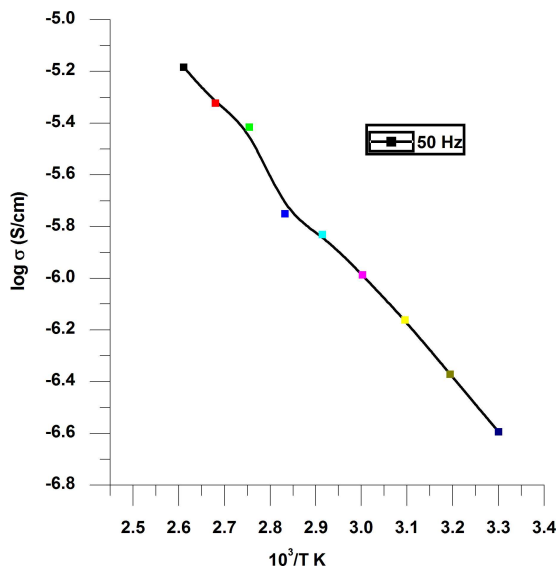


Fig. 7. Arrhenius plots of AC conductivity for $\text{LiNi}_{0.5}\text{Mn}_{0.5}\text{O}_2$ material.

The activation energies for AC conductivity at different temperature regions were obtained

by measuring the slope of the curves and using the Arrhenius relationship:

$$\sigma_{ac} = \sigma_0 \exp\left(-\frac{E_a}{k_B T}\right) \quad (4)$$

where σ_0 is a pre-exponential factor, E_a is the activation energy, k_B is Boltzmann's constant and T is the absolute temperature. The plots of $\log \sigma$ vs. $1000/T \cdot K$ are almost linear, obeying the Arrhenius relationship [44]. The activation energy for ionic conduction is found to be 0.281 eV for $\text{LiNi}_{0.5}\text{Mn}_{0.5}\text{O}_2$ compound at 50 Hz.

Table 3. AC conductivity values of $\text{LiNi}_{0.5}\text{Mn}_{0.5}\text{O}_2$ sample.

Temperature [°C]	AC conductivity [S/cm]
	$\text{LiNi}_{0.5}\text{Mn}_{0.5}\text{O}_2$
30	2.54×10^{-07}
40	4.24×10^{-07}
50	6.87×10^{-07}
60	1.03×10^{-06}
70	1.47×10^{-06}
80	1.78×10^{-06}
90	3.84×10^{-06}
100	4.75×10^{-06}
110	6.54×10^{-06}
120	3.52×10^{-06}

Fig. 7 shows AC conductivity values varying from 1.03×10^{-6} to 6.87×10^{-7} S/cm for $\text{LiNi}_{0.5}\text{Mn}_{0.5}\text{O}_2$ in the temperature range of 30 °C to 120 °C. The conductivity values are gradually increasing with increasing the temperature up to 120 °C. The AC conductivity values for $\text{LiNi}_{0.5}\text{Mn}_{0.5}\text{O}_2$ have been collected in Table 3 and the values are smaller than those found in other cathode materials. The low activation energy and low conductivity are attributed to a shrinking lattice effect. It is suggested that for smaller lattice dimensions, the decreasing size of the cavities, in which the lithium ions reside, brings these cations closer to M^{2+} ions. As a result, increased repulsion between Li^+ and M^{2+} reduces the strength of Li–O bonds resulting in lower activation energy and higher conductivity.

The dielectric constant ϵ' is calculated using the following relation:

$$\epsilon' = \frac{CL}{\epsilon_0 A} \quad (5)$$

where ϵ_0 is the permittivity of free space, C is capacitance, L is the thickness of the pellet, A is the effective area [45].

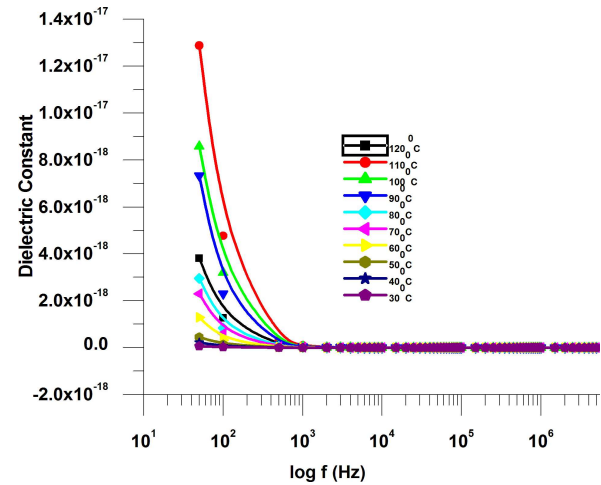


Fig. 8. Frequency variation of dielectric constant of $\text{LiNi}_{0.5}\text{Mn}_{0.5}\text{O}_2$ material at different temperatures.

From Fig. 8 it is observed that the dielectric constant (ϵ') decreases with increasing temperature, moreover, it rises sharply towards low frequencies and the shape of the rise is changing as the temperature increases. The increment of dielectric constant (ϵ') is rapid at lower temperatures and shows almost frequency independent behavior at higher temperature. At lower frequency regions, the dipoles get sufficient time to orient themselves completely along with the direction of the field, resulting in larger values of ϵ' of the sample [46].

The advantage of the electric modulus formalism is that it suppresses the information about electrode effects. This can also be used to study conductivity relaxation times. The complex modulus is defined as the inverse of the complex permittivity.

The impedance data were converted into electrical modulus by using the relation $M' = \omega C_0 Z'$ (real part) and $M'' = \omega C_0 Z''$ (imaginary part), where $C_0 = \epsilon_0 A/L$, A is the area of the sample, L is

the thickness of the sample and ϵ_0 is the permittivity of free space (8.854×10^{-14} F/cm) [47, 48]. The values are shown in Fig. 9.

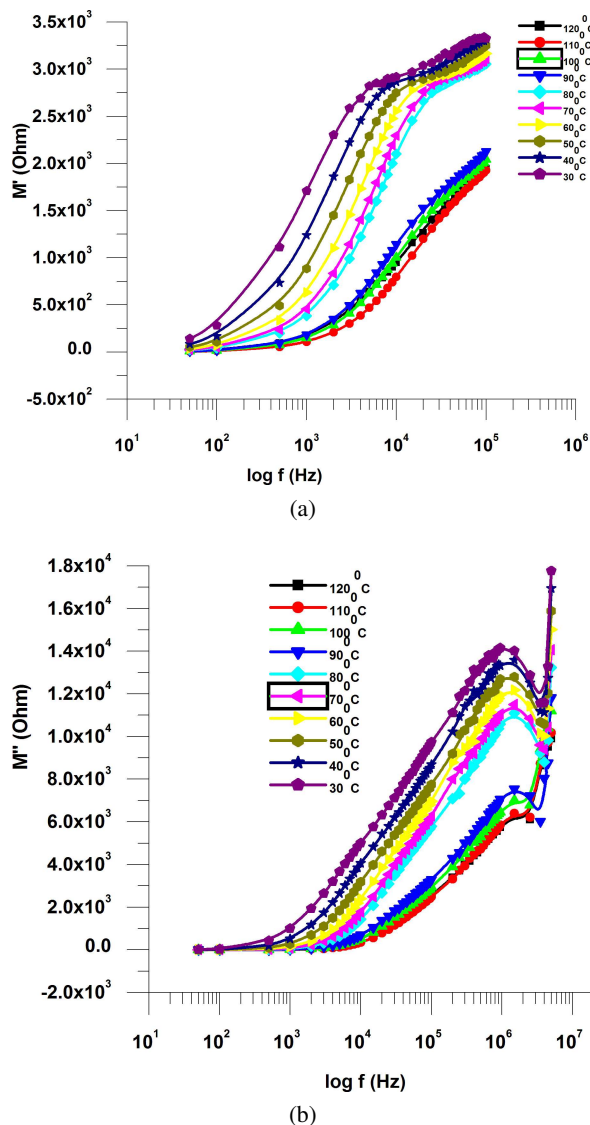


Fig. 9. (a) and (b): real and imaginary part of modulus for $\text{LiNi}_{0.5}\text{Mn}_{0.5}\text{O}_2$ material as a function of frequency at different temperatures.

Fig. 9a shows that M' values tend to a constant value at higher frequencies, whereas M'' has a peak centered at the dispersion point of M' . It is also clear from Fig. 9b that the value of M'' decreases and shifts toward higher frequencies as temperature increases. The variation of M' and M'' as a function of frequency shows shifting

of the peaks towards the high frequency as temperature increases, which implies that there is a distribution of ionic relaxation time. The shift in frequency of the M'' peak corresponds to the conductivity relaxation phenomenon [49].

4. Conclusion

In this work $\text{LiNi}_{0.5}\text{Mn}_{0.5}\text{O}_2$ material has been synthesized by sol-gel method at 800°C for 20 hours. The XRD and FESEM results indicate that the material is made of pure phase corresponding to layered $\alpha\text{-NaFeO}_2$ type structure and average particle size is around $10\ \mu\text{m}$. The FT-IR reveals that the local structure of the oxide lattice is constituted by LiO_6 and MO_6 octahedra. The impedance analysis of the material indicates the conductivity of the material and AC conductivity values which are found to be 6.54×10^{-6} . The AC conductivity obeys the Arrhenius law with activation energy $0.281\ \text{eV}$. The fitting data of EIS plots replicate the non-Debye relaxation process with negative temperature coefficient of resistance (NTCR) behavior.

References

- [1] OHZUKU T., MAKIMURA Y., *Chem. Lett.*, 30 (2001), 744.
- [2] PARK S.M., CHO T.H., YOSHIO M., *Chem. Lett.*, 33 (2004), 6.
- [3] ROSSEN E., JONES C.D.W., DAHN J.R., *Solid State Ionics*, 57 (1992), 311.
- [4] CAURANT D., BAFFLER N., BIANCHI V., GREGOIRE G., BACH S., *J. Mater. Chem.*, 6 (1996), 1149.
- [5] SPAHR M.E., NOVAK P., HAAS O., NESPER R., *J. Power Sources*, 68 (1997), 629.
- [6] LU Z., BEAULIEU L.Y., DONABERGER R.A., THOMAS C.L., DAHN J.R., *J. Electrochem. Soc.*, 149 (2002), A778.
- [7] WANG X., HAO H., LIU J., HUANG T., YU A., *Electrochim. Acta*, 56 (2011), 4065.
- [8] XIAO L., LIU X., ZHAO X., LIANG H., LIU H., *Solid State Ionics*, 192 (2011), 335.
- [9] MANIKANDAN P., ANANTH M.V., PREM KUMAR T., RAJU M., PERIYASAMY P., MANIMARAN K., *J. Power Sources*, 196 (2011), 10148.
- [10] LU Z., MACNEIL D.D., DAHN J.R., *Electrochem. Solid State Lett.*, 4 (2001), A191.
- [11] SHIN S.S., SUN Y.K., AMINE K., *J. Power Sources*, 112 (2002), 634.
- [12] K. MIZUSHIMA, JONES P.C., WISEMEN P.J., GOODENOUGH J.B., *Mater. Res. Bull.*, 15 (1980) 783.

- [13] NAGAURA T., OZAWA T., *Progr. Batteries Sol. Cells.*, 9 (1990), 20.
- [14] SPAHR M.E., NOVAK P., SCHNYDER B., HASS O., NESPER R., *J. Power Sources*, 68 (1997), 629.
- [15] MAKIMURA Y., OHZUKU T., *J. Power Sources*, 119 (1997), 156.
- [16] LU Z., MACNEIL D.D., DAHN J.R., *Electrochem. Solid State Lett.*, 4 (2001), A191.
- [17] LU Z., BAULIEU L.Y., DONABERGER R.A., THOMAS C.L., DAHN J.R., *J. Electrochem. Soc.*, 149 (2002), A778.
- [18] REED J., CEDER G., *Electrochem. Solid State Lett.*, 5 (2002), A145.
- [19] GREY C.P., YOON W.S., REED J., CEDER G., *Electrochem. Solid State Lett.*, 7 (2004), A290.
- [20] SPAHR M.E., NOVAK P., SCHNYDER B., HASS O., NESPER R., *J. Electrochem. Soc.*, 145 (1998), 1113.
- [21] *Unit-cell software for cell refinement method of tjb holland & sat redfern*, 1995.
- [22] LI D., SASAKI Y., KAGEYAMA M., KOBAYAKAWA K., SATO Y., *J. Power Sources.*, 148 (2005), 85.
- [23] LI D., MUTA T., NOGUCHI H., *J. Power Sources*, 135 (2004), 262.
- [24] LI D., NOGUCHI H., YOSHIO M., *Electrochim. Acta*, 50 (2004), 425.
- [25] SUN Y., OUYANG C., WANG Z., HUANG X., CHEN L., *J. Electrochem. Soc.*, 151 (2004), A504.
- [26] LU Z., MACNEIL D.D., DAHN J.R., *Electrochem. Solid State Lett.*, 4 (2001), A200.
- [27] MACNEIL D.D., LU Z., DAHN J.R., *J. Electrochem. Soc.*, 149 (2002), A1332.
- [28] JOUANNEAU S., MACNEIL D.D., LU Z., BEATTIE S.D., MURPHY G., DAHN J.R., *J. Electrochem. Soc.*, 150 (2003), A1299.
- [29] BIN Z., GANG C., PING X., ZUSHUN L., *Solid State Ionics*, 178 (2007) 1230.
- [30] SPAHR M.E., NOVAK P., SCHNYDER B., HAAS O., NESPER R., *J. Power Sources*, 68 (1997), 629.
- [31] MURALI N., VIJAYA B.K., EPHRAIM B.K., VEERAI AH V., *Chem. Sci. Trans.*, 3 (2014), 1317.
- [32] KANG K., MENG Y.S., BRÉGER J., GREY C.P., CEDER G., *Science*, 311 (2006), 977.
- [33] VENKATESWARA R.A., VEERAI AH V., PRASADA R.A.V., KISHORE B.B., VIJAYA K.K., *Ceram Int.*, 40 (2014), 13911.
- [34] DAS T., DAS B.K., PARASHAR K., PARASHAR S.K.S., NAGAMALLESWARA R.A., *Adv. Mat. Res.*, 938 (2014), 63.
- [35] MARTHA S.K., SCLAR H., FRAMOWITZ Z.S., KOVACHEVA D., SALIYSKI N., GOFER Y., SHARON P., GOLIK E., MARKOVSKY B., AURBACH D., *J. Power Sources*, 189 (2009), 248.
- [36] MURALI N., VIJAYA B.K., EPHRAIM B.K., VEERAI AH V., *AIP Conf. Proc.*, 1665 (2015), 140057-1.
- [37] SENTHIL K.P., SAKUNTHALA A., PRABU M., REDDY M.V., JOSHI R., *Solid State Ionics*, 267 (2014), 1.
- [38] SUN Y.K., MYUNG S.T., BANG H.J., PARK B.C., PARK S.J., SUNG N.Y., *J. Electrochem. Soc.*, 154 (2007), A937.
- [39] PRABAKARAN S.R.S., MICHAEL M.S., RADHAKRISHNAN S., JULIEN C., *J. Mater. Chem.*, 7 (1997), 1791.
- [40] PRABU M., SELVASEKARAPANDIAN S., KULKARNI A.R., HIRANKUMAR G., SANJEEVIRAJA C., *J. Rare Earth*, 28 (2010), P 435.
- [41] ROUT S.K., HUSSAIN A., SINHA E., AHN C.W., KIM I.W., *Solid State Sci.*, 11 (2009), 1144.
- [42] SAHOO P.S., PANIGRAHI A., PATRI S.K., CHOUDHARY R.N.P., *Bull. Mater. Sci.*, 33 (2010), 129.
- [43] PADHY R., RAO N., PARASHAR S.K.S., PARASHAR K., CHAUDHURI P., *Solid State Ionics*, 256 (2014), 29.
- [44] JHA P.A., JHA P.K., JHA A.K., DWIVEDI R.K., *Mater Res Bull.*, 48 (2013), 101.
- [45] KUMAR P., SINGH B.P., SINHA T.P., SINGH N.K., *Adv. Mater. Lett.*, 3 (2012), 143.
- [46] ORLIUKAS A., DINDUNE A., KANEPE Z., *Solid State Ionics*, 157 (2003), 177.
- [47] SAMBASIVARAO K., MADHAVA P.D., MURALI K.P., LEE J.H., *Physica B*, 403 (2008), 2079.
- [48] DRIDI N., BOUKHARI A., REAU J.M., ARBIB E., HOLT E.M., *Solid State Ionics*, 127 (2000), 141.
- [49] ROSAIAH P., HUSSAIN O.M., *Adv. Mat. Lett.*, 4 (2013), 288.

Received 2015-11-12

Accepted 2016-01-24